HERBSTEIN, F. H. (1961). *Advanc. Phys.* **10**, 313–355.
HUISZOON, C. & GRÖNEWEGEN, P. P. M. (1972). *Acta Cryst.* A**28**, 170–172.
JOSHI, S. & MITRA, S. (1960). *Proc. Phys. Soc.* **76**, 295–298.
KOUCHKOVSKY, R. DE (1974). *Acta Cryst.* A**30**, 406–408.
LANDOLT-BÖRNSTEIN (1969). *Numerical Data and Functions.* New series, group III, Vol. 2, p. 5. Berlin: Springer-Verlag.
MORLIN, Z. (1971). *Acta Cryst.* B**27**, 2493–2494.
SUORTTI, P. (1972). *J. Appl. Cryst.* **5**, 325–331.
VALLIN, J., BECKMAN, O. & SALAMA, K. (1964). *J. Appl. Phys.* **35**, 1222–1223.
WARREN, B. E. (1969). *X-ray Diffraction,* pp. 49, 56. Reading, Mass.: Addison-Wesley.
WASASTJERNA, J. A. (1946). *Soc. Sci. Fenn. Comm. Phys. Math.* **13**(5), 1–24.

Acta Cryst. (1974). A**30**, 413

Multiple Diffraction of X-rays and the Phase Problem. Computational Procedures and Comparison with Experiment*

BY R. COLELLA
Purdue University, Physics Department, W. Lafayette, Indiana 47907, *U.S.A.*

(*Received* 7 *November* 1973; *accepted* 14 *January* 1974)

The general theory of n-beam X-ray diffraction ($n>2$) has been developed in the framework of classical dynamical theory and applied to the Bragg case. It is shown that the crystal wave-vectors are the eigenvalues of a $4n\times 4n$ dispersion matrix. The boundary conditions are applied to a parallel-sided crystal slab and show that for an infinite thickness only $2n$ wave fields survive. The Umweganregung plot of Ge(222) with Cu $K\alpha$ radiation has been considered in detail. The integrated intensity of an Umweganregung peak is defined here as a double integral with respect to θ (angle of incidence) and φ (azimuthal angle). The 222–113 and 222–$\bar{1}\bar{1}3$ absolute integrated intensities were measured on a dislocation-free Ge crystal. Excellent agreement is obtained between experimental and calculated values. The ratio between the two integrated intensities (of the order of 7) did not change appreciably for a Ge mosaic crystal, although both reflections exhibited increases with respect to the perfect-crystal values. Since the two Umweganregung peaks considered in this experiment involve crystallographically equivalent reflections with different phases, it is suggested that the present technique can in principle be used for phase determination in crystal structure analysis.

Introduction

The inability to extract phase information in a diffraction experiment is commonly referred to as the 'phase problem'. A common statement frequently found in the literature is that only the magnitudes $|F_H|$ of the structure factors can be determined, essentially because present experimental techniques are able to measure intensities, not amplitudes. Indeed, when the restrictions imposed on the charge density $\varrho(\mathbf{r})$ are taken into account, the phase problem can be analytically solved, at least in principle (Karle, 1964). Mathematical complexities, however, frequently arise, especially in the case of non-centrosymetric crystals, so that we can still talk of a 'phase problem'.

The idea of extracting phase information from a scattering experiment is indeed one of the fundamental problems in metrology. This point has been discussed extensively by Goldberger, Lewis & Watson (1963), who also have made some interesting suggestions on how this could be done. The idea is to irradiate an object from two different, independent sources and measure simultaneously the correlation in the intensity fluctuations in the two detectors. It is interesting to note that one of the experiments proposed by these authors is based on multiple diffraction of X-rays.

A new physical method for phase determination has been recently proposed, in which use is made of recoilless nuclear resonance fluorescence of γ-radiation (Parak, Mössbauer, Biebl, Formanek & Hoppe, 1971). This method looks promising, although it is limited to crystals containing ^{57}Fe in their cell, or another suitable Mössbauer scattering center.

The fact that in multiple diffraction the intensities of the diffracted beams are affected by the relative phases of the structure factors involved was recognized long time ago (Lipscomb, 1949; Fankuchen & Ekstein, 1949). An intuitive consideration immediately suggests that this is the case. In fact in two-beam diffraction the crystal wave vectors, eigenvalues of the dispersion matrix, involve only the products $F_HF_{\bar{H}}$, which are real if absorption is neglected,† whereas in n-beam diffrac-

* Work supported by the National Science Foundation (MRL Program GH 33574).

† When absorption is important the products $F_HF_{\bar{H}}$ are no longer real and the phases do play some role on the intensities. This is the basis of a well known traditional method of phase determination.

tion the relation between eigenvalues and structure factors is more complicated, and the phases do not cancel out in general.

Multiple diffraction of electrons in relation to the phase problem has been treated in some detail by Kambe (1957).

The X-ray case has received comparably less attention, mainly because of inherent complexities associated with polarization effects and the boundary conditions. An attempt was made some years ago by Hart & Lang (1961) who observed the displacements of Pendellösung fringes when a third beam was excited in a Ge crystal. Their interpretation was based on an approximate theory obtained by adapting an electron diffraction dynamical theory to the X-ray case.

In recent years numerous treatments of multi-beam cases have appeared in the literature* (Saccocio & Zajac, 1965; Hildebrandt, 1967; Joko & Fukuhara, 1967; Ewald & Héno, 1968; Héno & Ewald, 1968; Penning, 1968; Penning & Polder, 1968; Dalisa, Zajac & Ng, 1968; Balter, Feldman & Post, 1971, and many others). In all these papers only the Laue case of diffraction was considered, because the authors' attention was concentrated on the enhancement of anomalous transmission occurring in some multi-beam cases (double Borrmann effect).

On the other hand, the Bragg case of diffraction is frequently used in multi-beam work, particularly when the azimuthal-scan technique is used. In this technique the crystal is rotated around the diffraction vector associated with a given set of lattice planes (*hkl*), and the angle of incidence θ is constant for the *hkl* reflection in the symmetric Bragg case. As the azimuthal angle φ is varied, it is possible that one or more nodes in reciprocal space lie on the Ewald sphere simultaneously with *hkl*, thus affecting the *hkl* intensity. These effects are very strong when the *hkl* reflection is weak, as observed by Renninger (1937) in the case of the 222 in diamond. This geometry looks favorable for studying phase effects, because the boundary conditions are the same for all the Umweganregung† peaks if the crystal surface is parallel to the (*hkl*) planes.

The (222) azimuthal plot of germanium with Cu $K\alpha$ radiation has been investigated in detail by Cole, Chambers & Dunn (1962). A glance at Fig. 6 of their paper immediately shows the importance of the phase effect. This figure reproduces in detail a portion of the 222 Umweganregung plot, and it is apparent that two crystallographically equivalent planes, (113) and ($\bar{1}\bar{1}3$), whose structure factors differ only by phase with respect to 222, produce peaks with different intensities. *This simple observation shows that a theory able to correlate structure factors with intensities in Umweganregung plots, if available, could be used for phase determination*, at least in principle.

* Only dynamical treatments are considered in this paper.

† 'detour radiation'. Name given by Ewald to the extra peaks observed by Renninger in diamond under the conditions of simultaneous diffraction.

Moreover, the Bragg case of diffraction is frequently used for accurate determination of structure factors *via* integrated intensities from perfect crystals. In these cases the occurrence of multiple reflections is usually considered a nuisance and suitable experimental conditions are sought in order to eliminate this effect There are situations, however, in which this is not possible or convenient, and one would like to make quantitative estimates. Although it is commonly accepted by crystallographers that weak reflections are more sensitive to multiple diffraction effects than strong reflections, there are no rigorous criteria, at present, for deciding which reflections can be affected by Umweganregung, especially in the case of perfect crystals. For instance, in the experimental part of this work no effect whatsoever (within 1%) was found in reflections such as 400, with Co $K\alpha$ radiation, in germanium. These considerations show that a detailed theoretical treatment of the problem is in order, with the specific aim of setting up a computational procedure for the Umweganregung peaks. Such a theory will be described in detail in the next section, and will then be compared with experiment.

2. Theory and computational methods: infinite crystal

In an infinite crystal the total wave field can be expressed as a superposition of vector plane waves, whose wave vectors are all related by reciprocal-lattice vectors [see, for instance, §§ III-8 and 9 of Zachariasen (1945)]. It is assumed that a finite, otherwise arbitrary, number n of waves are excited in the crystal corresponding to those nodes, in reciprocal space, that are very close or lie on the Ewald sphere. These nodes will be denoted as $H=1,2,\ldots,n$, with $H=1$ corresponding to the origin O.

When these plane waves are introduced into Maxwell's equations, the following set of simultaneous linear equations is obtained [see equation 3·105*b* of Zachariasen (1945)]:

$$(k_0^2-\beta_i^2)\mathbf{D}_i-\sum_{j=1}^{n}{}'\psi_{i-j}[(\boldsymbol{\beta}_i\cdot\mathbf{D}_j)\boldsymbol{\beta}_j-\beta_i^2\mathbf{D}_j]=0 \qquad (1)$$

where $k_0=1/\lambda$, λ is the wave length of X-rays in vacuum, $\boldsymbol{\beta}_j$ is the wave vector associated with the j node, $\mathbf{D}_j$ is the displacement vector amplitude and ψ_j is the Fourier component of the polarizability per unit volume (times 4π) associated with the same node. i can be equal to $1,2\ldots,n$ so that (1) really represents n linear homogenous equations for the amplitudes $\mathbf{D}_j$.

Equations (1) therefore represent a set of self-consistent conditions imposed on the plane waves excited in the crystal. Note that the O-beam, which will later be associated with the incident beam when the bounded crystal will be considered, does not play any privileged role. Its labelling merely corresponds to a particular choice of the origin in reciprocal space. Its existence is not assumed as due to an external incident

beam, which would be meaningless in view of the fact that we are considering an infinite crystal, but simply because we are *postulating* the existence of a set of waves coupled by diffraction. In other words, *if* a plane wave $\boldsymbol{\beta}_0$ exists in the crystal, a set of plane wave $\boldsymbol{\beta}_2, \boldsymbol{\beta}_3, \ldots, \boldsymbol{\beta}_n$ will also exist, whose wave vectors are related by

$$\boldsymbol{\beta}_j = \boldsymbol{\beta}_0 + \mathbf{B}_j \,, \tag{2}$$

$\boldsymbol{\beta}_j$ being reciprocal-lattice vectors, and whose amplitudes are related by equations (2).

Dividing by β_i^2 and rearranging some terms one obtains

$$[k_0^2/\beta_i^2 - (1-\psi_0)]\mathbf{D}_i - \sum_1^n{}'_j \psi_{i-j}[(\mathbf{u}_i \,.\, \mathbf{D}_j)\mathbf{u}_i - \mathbf{D}_j] = 0 \tag{3}$$

where the prime near the summation sign indicates that the term corresponding to $j=i$ is omitted, and $\mathbf{u}_i$ are unit vectors directed as $\boldsymbol{\beta}_i$.

At this point an assumption is introduced in traditional treatments of dynamical theory. Since β_i and k_0 are very close, differing only by a few parts in 10^{-5}, the first factor in brackets of equation (3) is usually written as $(\psi_0 - 2\delta_i)$ where $\delta_i + 1$ is the refractive index for the i wave. Since each δ_i can be linearly related to δ_0, the above process is equivalent to a linearization of the dispersion equations, that is to say, each equation (3) becomes a linear function of δ_0. In this process half of the solutions are thrown out of the problem, which is perfectly legitimate in most cases because these solutions correspond to plane waves of negligible intensity. This is not the case, however, when an intense diffracted beam is excited parallel to the surface, a situation not at all exceptional in multi-beam diffraction.* This point will be further clarified later on, when the boundary conditions will be discussed. We will therefore retain the first bracketed factor of (3) in its present form.

Every vector equation (3) gives rise, in principle, to three scalar equations. The displacement vectors $\mathbf{D}_j$, however, are bound to be normal to the wave vectors $\boldsymbol{\beta}_j$, which are fixed by the geometry of the crystal lattice. This restriction reduces the total number of scalar equations derived from (3) to $2n$. For every wave vector $\boldsymbol{\beta}_j$ we will consider two orthogonal unit vectors $\boldsymbol{\sigma}_j$ and $\boldsymbol{\pi}_j$, both normal to $\boldsymbol{\beta}_j$, defined in the following way:

$$\boldsymbol{\sigma}_j = \mathbf{u}_j \times \mathbf{u}_0 / |\mathbf{u}_j \times \mathbf{u}_0| \quad (j=2,3,\ldots,n) \tag{4}$$

$$\boldsymbol{\pi}_j = \mathbf{u}_j \times \boldsymbol{\sigma}_j \qquad (j=1,2,\ldots,n) \tag{5}$$

where $\mathbf{u}_j = \boldsymbol{\beta}_j/\beta_j$ and $\boldsymbol{\sigma}_0$ is arbitrarily chosen parallel to a particular direction normal to $\mathbf{u}_0$.†

When the ith equation (3) is scalarly multiplied by $\boldsymbol{\pi}_i$ and $\boldsymbol{\sigma}_i$ respectively ($i=1,2,\ldots,n$), the following set of scalar equations is obtained:

$$[k_0^2/\beta_i^2 - (1-\psi_0)]D_{i\pi} + \sum_1^n{}'_j \psi_{i-j}(D_{j\pi}\alpha_{ji}^{\pi\pi} + D_{j\sigma}\alpha_{ji}^{\sigma\pi}) = 0 \tag{6}$$

$$[k_0^2/\beta_i^2 - (1-\psi_0)]D_{i\sigma} + \sum_1^n{}'_j \psi_{i-j}(D_{j\pi}\alpha_{ji}^{\pi\sigma} + D_{j\sigma}\alpha_{ji}^{\sigma\sigma}) = 0 \tag{7}$$

where $D_{i\pi} = \mathbf{D}_i \,.\, \boldsymbol{\pi}_i$, $D_{i\sigma} = \mathbf{D}_i \,.\, \boldsymbol{\sigma}_i$, $\alpha_{ji}^{\pi\pi} = \boldsymbol{\pi}_j \,.\, \boldsymbol{\pi}_i$, $\alpha_{ij}^{\sigma\pi} = \boldsymbol{\pi}_i \,.\, \boldsymbol{\sigma}_j$, $\alpha_{ji}^{\sigma\sigma} = \boldsymbol{\sigma}_j \,.\, \boldsymbol{\sigma}_i$ and $\alpha_{ij}^{\sigma\pi} = \boldsymbol{\sigma}_i \,.\, \boldsymbol{\pi}_j$.

Equations (6) and (7) form a system of $2n$ homogeneous linear equations for the unknown amplitudes $D_{i\pi}$ and $D_{i\sigma}$. If we consider as variable the magnitude of the wave vector $\boldsymbol{\beta}_0$ (or its projection along an arbitrary direction), this system has nontrivial solutions if the determinant is zero, which gives rise to a discreet set of $4n$ eigenvalues β_0^i.*

The associated determinantal equation can be written:

$$|\mathsf{A} + \mathsf{T}| = 0 \tag{8}$$

Matrix A can be defined by means of four submatrices of n-order:

$$\mathsf{A} = \begin{pmatrix} \mathsf{P} & \mathsf{Q} \\ \mathsf{R} & \mathsf{S} \end{pmatrix}$$

where $P_{ii} = S_{ii} = \psi_0 - 1$, $Q_{ii} = R_{ii} = 0$, $P_{ij} = \psi_{i-j}\alpha_{ji}^{\pi\pi}$, $Q_{ij} = \psi_{i-j}\alpha_{ji}^{\sigma\pi}$, $R_{ij} = \psi_{i-j}\alpha_{ji}^{\pi\sigma}$, $S_{ij} = \psi_{i-j}\alpha_{ji}^{\sigma\sigma}$ $(i \neq j)$.

Matrix T is a diagonal matrix whose elements are: $T_{ii} = k_0^2/\beta_j^2$, with $j=i$ if $i=1,2,\ldots,n$, $j=i-n$ if $i=n+1,n+2,\ldots,2n$. We will now try to transform equation (8) in order to get a linear equation with respect to γ_0, projection of $\boldsymbol{\beta}_0$ along an arbitrary direction.†

Let us first consider the matrix X, inverse of A. If we multiply equation (8) by X (on the right side), and then by $\mathsf{T}^{-1} = \mathsf{C}$ (on the left side), we get

$$|\mathsf{C} + \mathsf{X}| = 0 \tag{9}$$

where $C_{ii} = \beta_i^2/k_0^2$ and $C_{ij} = 0$ $(i \neq j)$. Every term C_{ii} is a second-order polynomial in γ_0.

It can be shown that C can be written as a sum of three matrices:

$$\mathsf{C} = \gamma_0^2 \mathsf{I} + \gamma_0 \mathsf{C}_1 + \mathsf{C}_0 \tag{9'}$$

where C_1 and C_0 are diagonal matrices. Therefore the determinantal equation can be written as a second-order matrix polynomial:

$$|\gamma_0^2 \mathsf{I} - \mathsf{V}\gamma_0 + \mathsf{B}| = 0 \tag{10}$$

---

* Such a condition is frequently found, for example, in the 002 Umweganregung pattern of diamond structures. The strongest peak of the series, the 002–$\bar{1}11$, is in this category.

† In practical calculations $\boldsymbol{\sigma}_0$ was chosen parallel to the crystal surface.

* Strictly speaking, the α's are not constant quantities, since the directions $\mathbf{u}_j$ are affected by index of refraction effects. The same approximation is used in conventional two-beam dynamical theory (see, for instance, Zachariasen, 1945, p. 117).

† In practical calculations the inward normal to the entry surface of the crystal was chosen.

where I is the identity matrix, $V=-C_1$ and $B=C_0+X$.

It can be shown (see Appendix) that the solutions of equation (10) are the eigenvalues of a *linear* determinantal equation:

$$|Q-\gamma_0 I|=0 \qquad (11)$$

where Q is a $4n\times 4n$ matrix given by

$$Q=\begin{pmatrix} V & -B \\ I & O \end{pmatrix}$$

and O is the null matrix.

The problem of determining the eigenvalues of the dispersion equations (6) and (7) is therefore reduced to that of inverting the $2n\times 2n$ A matrix and diagonalizing the $4n\times 4n$ Q matrix. The eigenvalues can now be deter mined by means of standard methods for which computer programs are available.

The eigenvectors associated with equation (8) are also those of the system from which equations (9) and (10) are derived. It is shown in the Appendix that these eigenvectors are the first $2n$'s of those associated with equation (11).

The eigenvectors are usually provided by the same routine used for computing the eigenvalues and therefore the n-beam problem in the infinite crystal is completely solved. The various components of the displacement vectors $\mathbf{D}_i$ are determined only on a relative basis, however, because the dispersion equations (6) and (7) are homogeneous. There are $4n$ different sets of eigenvalues. Each set is normalized to unity ($\sum_1^n{}_j|\mathbf{D}_j^l|^2=1$, $l=1,2,\ldots,4n$). Each eigenvalue corresponds to a set of plane waves forming a wave field. In the infinite crystal the strength of every wave field has been arbitrarily set equal to one. In real cases, however, we will consider a finite crystal and the boundary conditions will determine the strengths of the various wave fields. More specifically, the total displacement vector in the crystal is written as:

$$\mathscr{D}(\mathbf{r})=\sum_1^{4n}{}_l q_l \sum_1^n{}_j \mathbf{D}_j^l \exp(-2\pi i\boldsymbol{\beta}_j^l)\,.\,\mathbf{r} \qquad (12)$$

where the q_l's are $4n$ unknown coefficients to be determined by means of the boundary conditions.

3. Theory and computational methods: boundary conditions

The boundary conditions for an electromagnetic wave propagating through the surface between two different media require continuity for the tangential components of the electric and magnetic intensities (**E** and **H**), and for the normal components of the electric displacement and magnetic induction (**D** and **B**). The latter conditions, however, are not independent from the former, so a total of four scalar equations are to be satisfied for each plane wave j [see, for instance, Jeans (1933)].

Ultimately, only the components of the displacement vectors will be involved in the final equations, through the relations:

$$\mathbf{H}_j=(k_0/\beta_j)\mathbf{u}_j\times\mathbf{D}_j$$
$$\mathbf{E}_j=(k_0^2/\beta_j{}^2)\mathbf{D}_j\,.$$

Let us consider a crystal slab of infinite lateral extent, finite thickness t, dividing the vacuum space into two regions, an 'upper' region where the incident, specularly reflected and diffracted beams are propagating, and a 'lower' region where only transmitted beams are travelling. In this treatment no distinction is made between Laue and Bragg beams, because such a distinction becomes meaningless for beams travelling almost parallel to the crystal surface. In this situation it may easily happen that within the same beam j, the associated plane waves $\boldsymbol{\beta}_j^l$ have positive or negative normal components, which makes it impossible to classify the j beam as a Bragg or Laue beam. For each beam j (other than the O beam) we will assume the existence of n vacuum *reflected* waves, travelling in the upper region and n vacuum *transmitted* waves, travelling in the lower region.†

For each beam j the associated reflected and transmitted waves have the same tangential components whereas the normal components differ only by sign. For the purpose of a physical interpretation of these vacuum waves, let us for a moment re-introduce the distinction between Bragg and Laue beams on an intuitive basis, neglecting the case of beams almost parallel to the crystal surface. For Bragg beams the reflected waves in the upper region are the diffracted waves and so are the transmitted waves in the lower region for Laue beams. Less clear is the physical meaning of the reflected waves associated with Laue beams and of the transmitted waves associated with Bragg beams. At this point we must recall that half of the solutions of the secular equation (8) correspond to waves whose amplitudes increase downwards into the crystal, whereas the other $2n$ waves have decreasing amplitudes. The same circumstance has been observed in treating the case of n-beam diffraction of high-energy electrons (Colella, 1972*a*; see § 4) and the reason for this is the same in the X-ray case. This is valid for *any* j beam, whether it is a Laue or Bragg beam, because all the wave vectors associated with the same eigenvalue have the same imaginary part. It is not unreasonable, therefore, to assume the existence of a reflected and transmitted wave for *any* j beam, whose wave vectors are defined by equations (13) and (14). The O beam is treated in the same way, except that in addition we have a beam travelling toward the crystal of unit amplitude (the incident beam). This treatment of the boundary

† Had we adopted a linearized form of the dispersion equations (see § 2), we would have a total of $4n$ unknowns in the problem: $2n$ ql's and $2n$ vacuum amplitudes. In such a situation we would be obliged to distinguish between Bragg and Laue beams, and would therefore be unable to handle the case of a j beam travelling parallel to the surface.

conditions is almost identical to that developed for n-beam electron diffraction (Colella, 1972*a*), the only difference being that in this case we have vector waves instead of scalar waves. [See also Lamla (1939).] Within the crystal the total electric displacement is described by equation (12). The vacuum wave vectors are given by:

$$\mathbf{k}_j^t = \mathbf{k}_0^t + \mathbf{B}_j^t \tag{13}$$

where $\mathbf{k}_0^t$ and $\mathbf{k}_j^t$ are the tangential components associated with the incident and diffracted waves, respectively, and $\mathbf{B}_j^t$ are the tangential components of reciprocal-lattice vectors. The normal components are fixed by the condition:

$$|\mathbf{k}_0| = |\mathbf{k}_j| = 1/\lambda \tag{14}$$

Within the crystal, for each beam j, there are in general $4n$ distinct directions given by the eigenvalues of the dispersion equations (6) and (7). Since there are four equations for each beam j on both surfaces of the crystal slab, we have a total of $8n$ equations with $8n$ unknowns: the $4n$ coefficients q_l in equation (12) and the $4n$ components of the electric displacement vectors projected on the entrance and exit surface of the crystal.

A linear system of simultaneous equations $8n \times 8n$ can therefore be written, whose solutions give at the same time the strengths q_l of the Bloch waves in the crystal and the amplitudes of the vacuum waves. Within each group of the four equations associated with the same beam j on each surface it is possible, however, to eliminate the two components of the electric displacement, so that ultimately we are left with a $4n \times 4n$ system whose unknowns are the q_l's.

(*a*) *O-Beam. Entrance surface*

$$\begin{aligned}\sum_l q_l D_{0\sigma}^l \left(\frac{1}{\varepsilon_0^l} + \frac{\sin\theta^l}{\sin\theta}\frac{1}{\sqrt{\varepsilon_0^l}}\right) &= \delta_\sigma \\ \sum_l q_l D_{0\pi}^l \left(\frac{1}{\sqrt{\varepsilon_0^l}} + \frac{\sin\theta^l}{\sin\theta}\frac{1}{\varepsilon_0^l}\right) &= \delta_\pi \,.\end{aligned} \tag{15}$$

In these equations $D_{0\pi}^l$ and $D_{0\sigma}^l$ are the normal and tangential components, respectively, of the crystal displacement vector associated with the lth wave field, $\sqrt{\varepsilon_0^l}$ is the lth dynamical refractive index, θ is the angle of incidence in vacuum and $\theta^l - \theta$ is the angular change due to refraction for the same wave field, δ_σ and δ_π are set equal to 2 and 0 for normal polarization, and to 0 and 2, respectively, for parallel polarization ('normal' and 'parallel' with respect to a plane defined by the normal $\mathbf{n}$ and the incident beam $\mathbf{k}_0$).

(*b*) *j-Beam. Entrance surface* ($j = 2, 3, \ldots, n$)

$$\sum_l q_l \left[D_{j\pi}^l \left(\frac{\pi_{jz}^l}{\varepsilon_j^l} + \frac{\sigma_{jx}^l}{\pi_{\bar{j}x}}\frac{1}{\sqrt{\varepsilon_j^l}}\right) + D_{j\sigma}^l \left(\frac{\sigma_{jz}^l}{\varepsilon_j^l} - \frac{\pi_{jx}^l}{\pi_{\bar{j}x}}\frac{1}{\sqrt{\varepsilon_j^l}}\right)\right] = 0 \tag{16}$$

$$\sum_l q_l \left[D_{j\pi}^l \left(\frac{\sigma_{jz}^l}{\sqrt{\varepsilon_j^l}} - \frac{\pi_{jx}^l}{\pi_{\bar{j}x}}\frac{1}{\varepsilon_j^l}\right) + D_{j\sigma}^l \left(-\frac{\pi_{jz}^l}{\sqrt{\varepsilon_j^l}} - \frac{\sigma_{jx}^l}{\pi_{\bar{j}x}}\frac{1}{\varepsilon_j^l}\right)\right] = 0 \,. \tag{17}$$

In these equations $D_{j\pi}^l$, $D_{j\sigma}^l$ and ε_j^l are the corresponding quantities, for the j beam, of those introduced in equations (13) and (14) for the O-beam. The lth dynamical index of refraction for the j beam is indicated as $\sqrt{\varepsilon_j^l}$, and π_{jz}^l, π_{jx}^l, σ_{jz}^l, σ_{jx}^l are components of two sets of unit vectors $\boldsymbol{\pi}_j^l$ and $\boldsymbol{\sigma}_j^l$ along two orthogonal directions $\mathbf{x}$ and $\mathbf{z}$ parallel to the crystal surface. For each beam j a set of directions $\mathbf{u}_j^l$ ($= \boldsymbol{\beta}_j^l/\beta_j^l$) can be defined using equation (2) if the angle of incidence θ and the eigenvalues of equation (11) are known. The two unit vectors $\boldsymbol{\pi}_j^l$ and $\boldsymbol{\sigma}_j^l$ are mutually perpendicular, both normal to $\boldsymbol{\beta}_j^l$, and defined by the following relations (for convenience):

$$\begin{aligned}\boldsymbol{\sigma}_j^l &= \mathbf{u}_j^l \times \mathbf{u}_0^l / |\mathbf{u}_j^l \times \mathbf{u}_0^l| \\ \boldsymbol{\pi}_j^l &= \mathbf{u}_j^l \times \boldsymbol{\sigma}_j^l \,.\end{aligned} \tag{18}$$

The z axis is chosen to be normal to the plane defined by $\mathbf{k}_i^t$ and $\mathbf{n}$ (unit normal to the crystal surface pointing inward), so that the choice of the x and z axes is different for each j beam. $\pi_{\bar{j}x}$ is the x projection of a unit vector $\boldsymbol{\pi}_{\bar{j}}$, normal to the z axis and to a vacuum wave vector $\mathbf{k}_{\bar{j}} = \mathbf{k}_j^t - \mathbf{n}(1/\lambda^2 - k_j^{t2})^{1/2}$.†

(*c*) *O-Beam. Exit surface*

$$\begin{aligned}\sum_l q_l C^l D_{0\sigma}^l \left(\frac{1}{\varepsilon_0^l} - \frac{\sin\theta^l}{\sin\theta}\frac{1}{\sqrt{\varepsilon_0^l}}\right) &= 0 \\ \sum_l q_l C^l D_{0\pi}^l \left(\frac{1}{\sqrt{\varepsilon_0^l}} - \frac{\sin\theta^l}{\sin\theta}\frac{1}{\varepsilon_0^l}\right) &= 0\end{aligned} \tag{19}$$

where $C^l = \exp(-2\pi i \gamma_0^l t)$ and γ_0^l are the normal components of the crystal O-beam, eigenvalues of the secular equation (8).

(*d*) *j-Beam. Exit surface* ($j = 2, 3, \ldots, n$)

$$\sum_l q_l C^l \left[D_{j\pi}^l \left(\frac{\pi_{jz}^l}{\varepsilon_j^l} - \frac{\sigma_{jx}^l}{\pi_{\bar{j}x}}\frac{1}{\sqrt{\varepsilon_j^l}}\right) + D_{j\sigma}^l \left(\frac{\sigma_{jz}^l}{\varepsilon_j^l} + \frac{\pi_{jx}^l}{\pi_{\bar{j}x}}\frac{1}{\sqrt{\varepsilon_j^l}}\right)\right] = 0 \tag{20}$$

$$\sum_l q_l C^l \left[D_{j\pi}^l \left(\frac{\sigma_{jz}^l}{\sqrt{\varepsilon_j^l}} + \frac{\pi_{jx}^l}{\pi_{\bar{j}x}}\frac{1}{\varepsilon_j^l}\right) + D_{j\sigma}^l \left(-\frac{\pi_{jz}^l}{\sqrt{\varepsilon_j^l}} + \frac{\sigma_{jx}^l}{\pi_{\bar{j}x}}\frac{1}{\varepsilon_j^l}\right)\right] = 0 \,. \tag{21}$$

The set of equations (15), (16), (17), (19), (20) and (21) form a set of $4n$ linear equations with $4n$ unknowns (the q_l's). The intensities of the various waves can therefore be determined by solving this system. It can be shown that for ordinary thicknesses ($t \simeq 1$ mm) half

† When the radicand is negative, $\mathbf{k}_{\bar{j}}$ corresponds to a beam whose intensity is extinguished a few Å away from the surface

of the q_l's vanish, and that the equations on the exit surface do not need to be considered. The method of elimination is entirely analogous to that described in the case of electron diffraction (Colella, 1972*a*; § 4) and will not be repeated here. With X-rays, however, the absorption is not so high as in the case of electron diffraction, and we are not considering only diffraction at glancing angle. This means that in the X-ray case we may have to retain some of the equations (19), (20) and (21). If the eigenvalues are ordered in such a way that their imaginary parts are in increasing order,* a careful analysis will show that: (i) the number k of non-vanishing q_l's ($2n \le k \le 4n$) depends on whether or not the ratio C^{k+1}/C^k exceeds a certain value, say exp (15); (ii) the number $l_{\max}$ of non-zero q_l's is determined by computing the ratio C^{k+1}/C^k for $k=2n,\ 2n+1,\ 2n+2,\ \ldots,\ 4n$; (iii) when this ratio is found greater than exp (15) $l_{\max}$ is set equal to k. Except for a few particular cases of very thin crystals, $l_{\max}$ has always turned out to be equal to $2n$. Once the q_l's are determined, the boundary conditions on the entrance surface for the j vacuum reflected amplitude give:

$$\mathscr{D}_{\bar{j}\pi} = \sum_l q_l (D^l_{j\pi}\sigma^l_{jz} - D^l_{j\sigma}\pi^l_{jz}) \,.\, (\varepsilon^l_j)^{-1/2}$$
$$\mathscr{D}_{\bar{j}\sigma} = \sum_l q_l (D^l_{j\pi}\pi^l_{jz} + D^l_{j\sigma}\sigma^l_{jz}) \,.\, (\varepsilon^l_j)^{-1} \qquad (22)$$

where $\mathscr{D}_{\bar{j}\pi}$ and $\mathscr{D}_{\bar{j}\sigma}$ are the parallel and perpendicular components, respectively, of the j reflected beam in vacuum (the plane of reference is defined by the normal $\mathbf{n}$ and the reflected beam $\mathbf{k}_{\bar{j}} = \mathbf{k}^t_j - \mathbf{n} \,.\, (\lambda^{-2} - k^{t2}_j)^{1/2}$. The intensity is given by: $I_{\bar{j}} = |\mathscr{D}_{\bar{j}\pi}|^2 + |\mathscr{D}_{\bar{j}\sigma}|^2$. Two sets of q_l's are determined, for the two polarization states of the incident beam. The final intensity of the j beam is given by:

$$I_{\bar{j}} = \alpha_{\text{perp}} I^{\text{perp}}_{\bar{j}} + \alpha_{\text{par}} I^{\text{par}}_{\bar{j}} \qquad (23)$$

where α_{perp} and α_{par} are the fractions of perpendicular and parallel components, respectively, of the incident beam. When the boundary conditions are applied on the exit surface, equations similar to (22) are obtained for the vacuum Laue diffracted beams.

4. Experimental procedures and comparison with theory

In comparing theory with experiment, one is tempted to use the theory described in the previous two sections in order to reproduce an azimuthal plot such as that obtained by Cole, Chambers & Dunn (1962). One major difficulty, however, becomes immediately apparent. Each point of an experimental azimuthal plot is referred, in principle, to particular, well defined values of the angle of incidence θ and the azimuth φ. In practice, however, because of the finite divergence of the incident beam, each point should be more properly referred to finite intervals of θ and φ values over which the n-beam reflectivity is integrated. Such integrations involve the structure of the incident beam (intensity as a function of θ and φ) which is difficult to evaluate. *A more precise way of characterizing an azimuthal plot seems to describe the intensity of each peak by a number which represents a doubly integrated intensity over θ and φ.* By 'integrated intensity' we will mean therefore, from now on, the following dimensionless quantity:

$$R(^{h'k'l'}_{hkl}) = \int\int I_{\bar{j}}\,(\theta,\varphi)\mathrm{d}\theta\mathrm{d}\varphi \qquad (24)$$

where $I_{\bar{j}}\,(\theta,\varphi)$ has been defined by equation (23) and the Miller indices in parentheses indicate the two beams excited simultaneously with 000. The three-beam case only has been considered in comparing theory with experiment because it is the most suitable for phase identification and the computing time is reasonable.

(*a*) *Experimental.* 222–113 *and* 222–$\overline{1}$13 *integrated intensities*

A double-crystal spectrometer in the antiparallel arrangement was used in this experiment. Both crystals were cut parallel to the (111) planes within 10 minutes of arc from a *p*-type germanium ingot† with an impurity concentration inferior to 10^{16} cm^{-3}, as measured by Hall effect at 77 °K. The crystals were ground with 400–600–1200 and 3200 SiC powders on glass and etched for 3–4 min in CP4 (5 parts HNO_3, 3 parts HF, 3 parts of acetic acid and 0·06 parts of bromine) at room temperature. No dislocation pits were visible after etching. The first crystal was diffracting in the 333 position and a slit was positioned between the two crystals so that $K\alpha_2$ was eliminated and the vertical divergence (normal to the diffraction plane) was of the order of 30′. A proportional counter with single-channel analyzer was used in order to discriminate against high-energy harmonics. Absolute values of integrated intensities were obtained by measuring the power of the X-ray beam after the first crystal by means of calibrated filters. Cu $K\alpha$ radiation was used throughout these experiments.

The quality of crystal perfection was checked by comparing the 333–$\overline{333}$ rocking curve with a theoretical profile obtained using dynamical theory. The integrated intensity of the rocking curve differed from the theoretical value by 2–3%, but the width was different for various regions of both crystals, ranging from the theoretical value ($\simeq 6''$) to 7·5″. This is an indication that our dislocation free crystals still contained some kind of imperfections, probably slight inhomogeneities in impurity concentration.

When the integrated intensity of 'Umweganregung' peaks is to be compared with theoretical values, the 'true' 222 is involved in the calculations. This forbidden reflection was therefore measured in absence of simultaneous reflections, and its value was found to

* The ordering procedure here is opposite to that described in (Colella, 1972*a*) because of a different sign in the exponents of the Bloch waves.

† Manufactured by Texas Instruments Inc., Dallas, Texas. The author is indebted to Professor S. Moss who kindly provided the Ge single crystal.

be $1{\cdot}79\times10^{-8}$, consistent with a structure factor $F_{222}=1{\cdot}09$. A similar value (1·18) was found by Renninger (1960).

An absolute measurement of the 'Umweganregung' peak (222–113), the most intense of the azimuthal plot, was made by measuring several rocking curves (intensity *vs.* θ, angle of incidence) for different values of φ, azimuthal angle. The second crystal was rotated by increments of 3·33′ over an interval $\Delta\varphi$ of 53·3′ centered on an average φ_0 value corresponding to full excitation of the simultaneous reflection 113. The results are shown in Fig. 1, where R^θ, the integrated intensity with respect to θ, is plotted as a function of φ. The tails of this profile tend asymptotically to the 'true' 222 value ($1{\cdot}79\times10^{-8}$). The area of this profile is the integrated intensity of this 'Umweganregung' peak as defined by equation (24). The points are measured values and the continuous line is an arbitrary interpolation. Two such measurements were performed in different experimental conditions of alignment and divergence slits. The R^θ plots were quite different, but the areas differed only by 1·6%. Integrating over φ is essentially equivalent to integrating over the vertical divergence of the beam. In this way the integrated intensity we arrive at is independent of the structure of the incident beam, and truly represents a number which can be compared with theory.

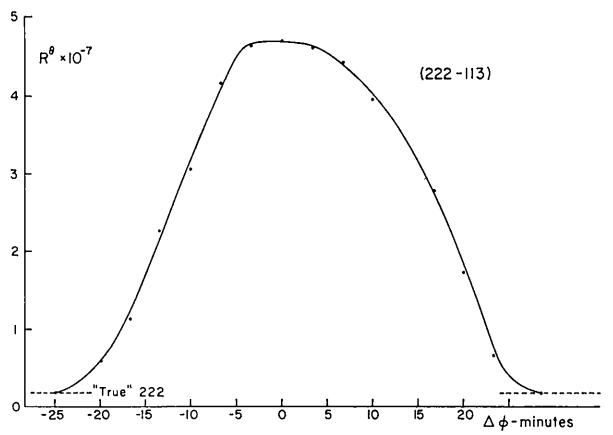

Fig. 1. Experimental integrated intensity of the 222 reflection as a function of the azimuthal angle. Each point of this profile represents an integration of the crystal reflectivity with respect to θ, angle of incidence. Points are experimental values, whereas the continuous line is an arbitrary interpolation. The tails tend asymptotically to the 'true' 222 value. The abscissa $\Delta\varphi=0$ has been arbitrarily set at the peak center. It corresponds to full excitation of the 113 simultaneous reflection.

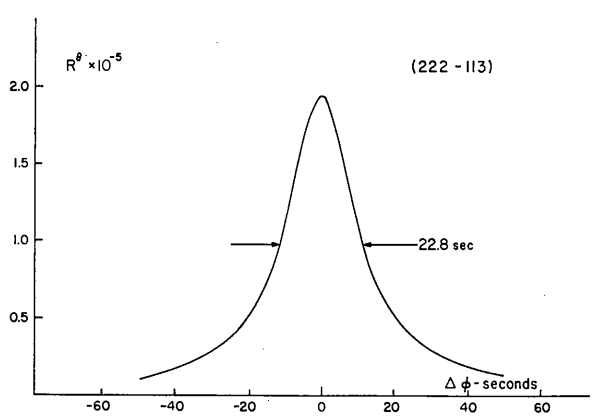

Fig. 2. Calculated integrated intensity of the 222 reflection as a function of the azimuthal angle. Each point of this profile represents an integration of the crystal reflectivity with respect to θ, angle of incidence. The tails tend asymptotically to the 'true' 222 value, which is a negligible fraction of the peak value. The abscissa $\Delta\varphi=0$ corresponds to full excitation of the 113 simultaneous reflection, as obtained from a kinematic calculation.

The same procedure could not be adopted for the 222–$\overline{1}\overline{1}3$. This reflection is much weaker than the 222–113, and a R^θ *vs.* φ plot would have been too time consuming. It was decided, therefore, that a relative measurement could be adequate for this work. The vertical divergence of the incident beam (of the order of 30′) was much greater than the intrinsic azimuthal width $\Delta\varphi$ over which the third beam (113 or $\overline{1}\overline{1}3$) was fully excited. This was proved experimentally by noting the broad flat maximum in the R^θ *vs.* φ plot for the 222–113 peak. We may conclude by way of extrapolation that this statement is certainly true also for the 222–$\overline{1}\overline{1}3$ peak which is much weaker. The calculations have confirmed this assumption for both reflections (see Figs. 2 and 3).

With this assumption in mind, an integrated intensity (over θ) measured at $\varphi=\varphi_0$ corresponding to the center of the flat maximum in the R^θ *vs.* φ plot is *proportional to a doubly integrated intensity, with respect to* θ *and* φ. *In this way any other 'Umweganregung' peak can be measured at one single* φ *value and put on an absolute basis by comparing with the* 222–113.

(*b*) *Theory.* 222–113 *and* 222–$\overline{1}\overline{1}3$ *integrated intensities*

Calculated values for the 222–113 and 222–$\overline{1}\overline{1}3$ could be obtained by computing several rocking curves (*I vs.* θ) at different φ values, and then evaluating the area of similar R^θ *vs.* φ plots (see Figs. 2 and 3). It is interesting to consider in detail a few of these *I vs.* θ plots. Fig. 4 shows two 222–113 *I vs.* θ plots, at two different values of φ. Note the high value of the maximum reflectivity at $\Delta\varphi=0$* ($I=0{\cdot}59$), and how the area under the peak is reduced by a small azimuthal rotation ($\Delta\varphi=15{\cdot}5''$). Fig. 2 shows that the full width at half height of the R^θ *vs.* φ plot amounts to 23 seconds of arc, for the 222–113 combination. These features are more or less common to all of the 'Um-

* $\Delta\varphi=0$ means $\varphi=\varphi_0$ where φ_0 is the azimuth at which the 113 node lies exactly on the Ewald sphere. φ_0 was calculated using a kinematic procedure similar to that described by Cole, Chambers & Dunn (1962). Cases have been found (other than the 222–113 combination) where the fullest multibeam excitation was found for $\Delta\varphi$ slightly different from 0 (see Fig. 3). This is not surprising because we are using a dynamical theory and refraction effects are included.

weganregung' peaks investigated. The $\Delta\varphi=0$ profile has an integrated intensity (over θ) comparable to that of a 'normal' strong reflection. These considerations lead us to conclude, therefore, that the 'Umweganregung' peaks are much weaker than the 'normal' reflections *only because the conditions for multibeam excitation are fulfilled within a very narrow range of the vertical divergence.* This circumstance had been previously pointed out in connection with neutron diffraction work (Colella, 1972*b*) and explains why multiple diffraction effects are negligible, in neutron and X-ray diffraction, when the primary reflection (the 222 in this experiment) is strong. Of course this is not the case in our experiment.

Fig. 4 shows that for $\Delta\varphi\neq 0$ the profile splits into two peaks, which is not surprising in view of the fact that with three beams interacting in the crystal two resonance errors are involved. It has been noted in all our multi-beam calculations that in general, for $\Delta\varphi\neq 0$, the I *vs.* θ profiles always consist of two peaks, one centered at the same value θ_0 close to the kinematic value θ_B (as given by Bragg's law without refraction effects), the other one located at a θ value such that the distance $\Delta\theta=\theta-\theta_0$ is approximately proportional to $\Delta\varphi$ ($\Delta\theta$ changes sign with $\Delta\varphi$). As $|\Delta\varphi|$ increases, both peaks shrink and eventually flatten down to negligible values. Since it is impractical to calculate integrated intensities R^θ for large $|\Delta\varphi|$, some sort of extrapolation procedure should be designed for extending the tails of the R^θ *vs.* φ plots to $\pm\infty$, thereby minimizing truncation errors. It has been found empirically that a Lorentzian profile [$R^\theta\simeq K/(\lambda+\varphi^2)$] is a fairly good approximation for large φ values, so that the areas under the tails can be evaluated analytically.

The results are summarized in Table 1 where the absolute values of the 222–113 peak and the ratios between the 222–113 and 222–$\overline{1}\overline{1}3$ integrated intensities are shown. It can be seen that the agreement between experimental and calculated values is excellent, and this is taken as a sufficient test of correctness for our theoretical and computational procedures.

Table 1. *Experimental and calculated integrated intensities of the* 222–113 *and* 222–$\overline{1}\overline{1}3$ *Umweganregung peaks* (*see definition in* § 4)

The ratios between the integrated intensities of two different Umweganregung peaks are listed in the right column.

		Ratio
Integrated intensities	222–113	222–113/222–$\overline{1}\overline{1}3$
Experiment	$3{\cdot}86\times10^{-9}$	7·48
Theory	$3{\cdot}67\times10^{-9}$	7·28

(*c*) *Experimental.* 222–113 *double-crystal rocking curve*

As a further test of our multi-beam theory, the double-crystal rocking curve 222–113 has been investigated. In this experiment the two Ge (111) crystals are set parallel for the 222 forbidden reflection, their azimuths being adjusted in order to produce the 113 simultaneous reflection. The beam diffracted by the first crystal had a negligible vertical divergence (less than 1′) because the conditions for multiple diffraction are satisfied only within a very small range of the vertical divergence, as noted in the previous paragraph.

The total power carried by this beam, with a cross section of approximately 1 mm², was of the order of 5000 photons $\sec^{-1}$ with 30 kV and 25 mA.

It is suggested that such a monochromator could be used in applications where a very small vertical divergence is required. An equivalent arrangement, in which two Ge crystals were used, was proposed by Williamson & Fankuchen (1959). In our experiment the two crystals are, so to speak, built in the same monolithic Ge crystal, because we exploit simultaneous diffraction from different Bragg planes.†

† A suggestion to use multiple diffraction in order to obtain parallel beams of neutrons was made by Kottwitz (1971).

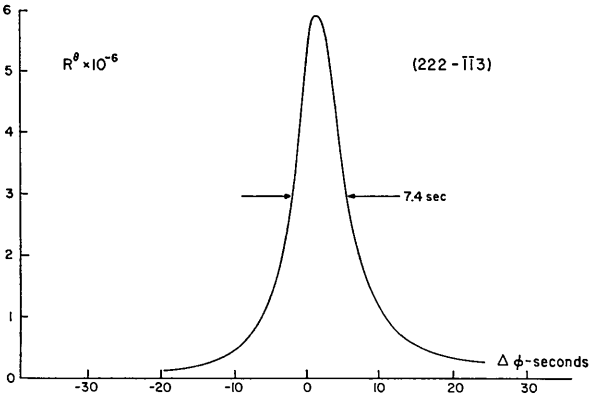

Fig. 3. Same as Fig. 2. except that the simultaneous reflection is now $\overline{1}\overline{1}3$. Note that full excitation occurs for $\Delta\varphi\neq 0$.

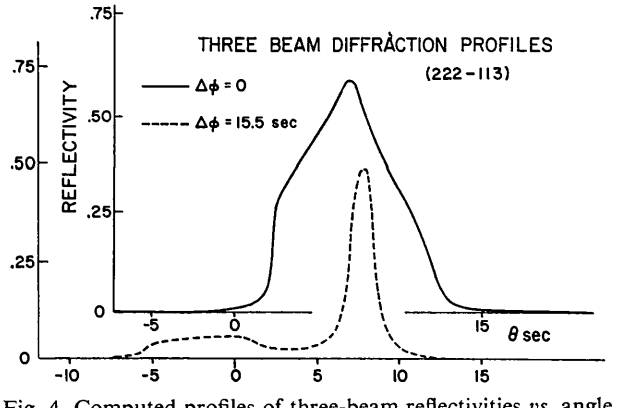

Fig. 4. Computed profiles of three-beam reflectivities *vs.* angle of incidence, for two different values of the azimuthal angle. $\Delta\varphi=0$ corresponds to full excitation of the 113 simultaneous reflection. The abscissa $\theta=0$ corresponds to the Bragg angle, without refraction correction, for the 'true' 222.

The anti-parallel arrangement was used, in order to eliminate any broadening due to non-monochromaticity of the X-ray source. Great care was exercised in the azimuthal orientation of the second crystal. The adjustment had to be done with an accuracy better than one minute of arc, owing to the small divergence of the incident beam. For the same reason, the tilting of the second crystal [rotation around an axis parallel to the (111) lattice planes and the diffraction plane] did not play any role in the half-width of the rocking curve, as opposed to what happens in a conventional double-crystal spectrometer. The peak intensity, after diffraction from the second crystal, was of the order of 10^3 counts $\sec^{-1}$.

It can be easily shown, by extending the ordinary two-beam theory of a double crystal spectrometer [see, for instance James (1965)], that the 222–113 rocking curve can be expressed by:

$$F(\beta)=\frac{R^{\mathrm{perp}}(\beta)+R^{\mathrm{par}}(\beta)}{R_0^{\mathrm{perp}}(\beta)+R_0^{\mathrm{par}}(\beta)} \tag{25}$$

where β is the angular position of the second crystal, F is the intensity reflected by the second crystal, and:

$$R(\beta)=\iint I(\alpha,\varphi)I(\alpha-\beta,\varphi)\mathrm{d}\alpha\mathrm{d}\varphi$$

$$R_0(\beta)=\iint I(\alpha,\varphi)\mathrm{d}\alpha\mathrm{d}\varphi \tag{26}$$

where α and φ are to be integrated between $-\infty$ and $+\infty$, and $I(\alpha,\varphi)$ is the 222–113 reflectivity function as defined by equation (23) for a given polarization. In deriving equations (25) and (26) the change in the angle of incidence θ due to a small change of the azimuthal angle φ has been neglected, as in the ordinary two-beam theory (James, 1965).

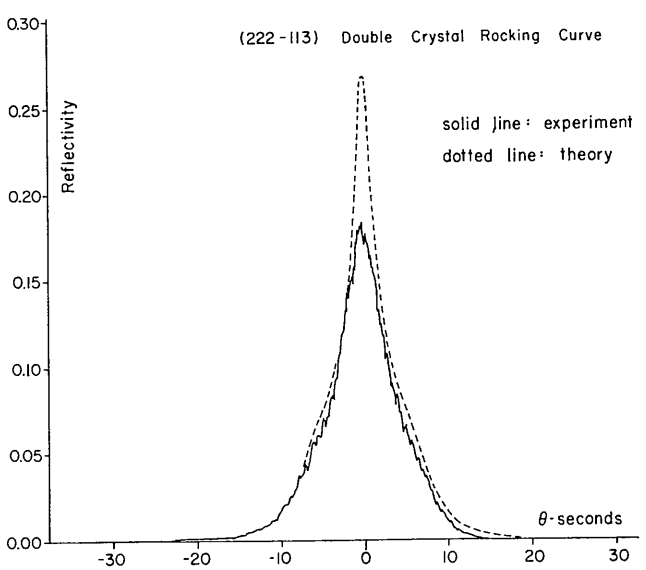

Fig. 5. Double-crystal rocking curve of the 222–113 three-beam reflection, using the anti-parallel arrangement. Both crystals are set for the 222, their azimuths being adjusted for simultaneous excitation of the 113.

The rocking curve $F(\beta)$ (equation 25) has been evaluated using the same I *vs.* θ profiles at different φ's used in deriving the diagrams presented in Figs. 2 and 3. The result is shown in Fig. 5. The agreement between theory and experiment is remarkably good, except in a narrow interval centered on the peak region. The experimental integrated intensity is about 10% smaller than the calculated value. No satisfactory explanation has been found for this discrepancy, except the fact that the experimental peak intensity was critically dependent on the φ adjustment. Since the mechanical accuracy of the azimuthal adjustment was of the order of $\pm 30''$, whereas it is known that an azimuthal misorientation of $11''$ is sufficient to halve the R^θ integrated intensity (see Fig. 2), it is not unreasonable to attribute the discrepancy between the peak values in Fig. 4 to azimuthal maladjustment. Given the complexities inherent in the experimental and computational aspects of this experiment, we feel that theory and experiment are in substantial agreement.

(d) Effects of lattice imperfections

The present theory is valid only for perfect crystals. Since ordinary crystals used in crystal structure determination are not as perfect as germanium, one might wonder to what extent is n-beam dynamical theory applicable to real crystals. To check this point the surface of the germanium sample was deliberately damaged by grinding with 120–240–400–600 SiC powders. The 333 double-crystal rocking curve in the anti-parallel arrangement was repeated for comparison with previous results obtained after etching. The full width at half maximum turned out to be $97''$ (instead of $6{\cdot}6''$ as previously measured) and the integrated intensity was found $5{\cdot}69\times10^{-5}$, to be compared with the perfect crystal value: $2{\cdot}08\times10^{-5}$ and the mosaic value: $8{\cdot}09\times10^{-5}$. Owing to the relatively small mosaic spread introduced ($\simeq 2'$) as compared with the vertical divergence of the incident beam ($\simeq 30'$), it can still be assumed that an integrated intensity (with respect to θ) measured at some central value φ_0 of the azimuth represents an integration with respect to φ as well. Therefore, one single integrated intensity for each Umweganregung peak measured at $\varphi=\varphi_0$ represents a relative value directly comparable with the values presented in Table 1. It was found that the 222–113 peak increased by a factor of about 8, whereas the ratio between 222–113 and 222–$\overline{1}$13 increased by 2. This shows that the *ratio* between Umweganregung peaks is much less sensitive to lattice imperfections than the peaks themselves.

We believe that ordinary crystals used in crystal structure determination are more dynamical for low $\sin\theta/\lambda$ reflections than our Ge crystal ground with SiC powder. In fact situations frequently arise when im-

perfections are deliberately introduced to make crystals more kinematic, by immersion in liquid nitrogen, for example. Therefore, it is not unrealistic to think of applying the present n-beam dynamical theory to complex organic or biological crystals.

5. Conclusions

It is pointed out that phase information can be obtained from multiple diffraction effects. More specifically, the phase of a hkl reflection relative to another $h'k'l'$ reflection affects the intensities of both when they are excited simultaneously. A general theory for the computation of n-beam integrated intensities has been developed and adapted to the Bragg case. It is found that the approximations leading to linearization of the dispersion matrix in ordinary two-beam dynamical theory are not valid in the n-beam case when one or more of the diffracted beams propagate almost parallel to the crystal surface. If n beams are excited, therefore, there are $4n$ wave fields, of which only $2n$ survive in the infinite crystal. The two different states of polarization lead to two distinct sets of boundary conditions. A computer program has been developed for computing n-beam reflectivities as a function of θ, the angle of incidence, and φ, the azimuthal angle. It is found in this work that the best way to compare theory with experiment is to consider doubly integrated intensities, with respect to θ and φ.

The 222 azimuthal plot of germanium is considered in detail. Calculations and experimental measurements have been carried out for the 222–113 and 222–$\overline{1}\overline{1}3$ Umweganregung peaks, whose integrated intensities differ by a factor of seven approximately. Since these two peaks involve crystallographically equivalent reflections, the intensity difference is due to the different phases of 113 and $\overline{1}\overline{1}3$ with respect to 222. Substantial agreement is found between theory and experiment. Conceivably, the present theory could be used to sort out phases from n-beam intensities. Since ordinary crystals are not as perfect as germanium the effect of lattice imperfections has been investigated by repeating the same measurements on a heavily damaged surface. It was found that, although the two integrated intensities were greatly increased, their ratio did not change by more than a factor of 2. Since most of the crystals used in crystal structure determination exhibit severe extinction effects for low-order reflections, it is suggested that the *ratio* between integrated intensities of Umweganregung peaks can be used for phase identification in X-ray diffraction.

Thanks are due to Professor S. Moss who kindly provided the dislocation-free Ge crystal. This work was supported by the National Science Foundation, Materials Research Laboratory Program, Grant GH 33574. A substantial amount of computing time was made available by the Computing Center at Purdue University.

APPENDIX

The proof is entirely analogous to that used in ordinary algebra for determining the roots of an n-order polynomial by diagonalizing the associated n-order matrix.

We will proceed backwards. Let us consider a 2×2 linear system of first order homogeneous equations:

$$\begin{pmatrix} \mathsf{V} & -\mathsf{B} \\ \mathsf{I} & \mathsf{O} \end{pmatrix} \begin{pmatrix} \mathsf{X}_1 \\ \mathsf{X}_2 \end{pmatrix} = \mu \begin{pmatrix} \mathsf{X}_1 \\ \mathsf{X}_2 \end{pmatrix} \qquad \text{(A-1)}$$

where μ is a complex number, and all other symbols denote matrices of $2n$-order. V, $-\mathsf{B}$, I and O are square matrices, whereas X_1 and X_2 are single column matrices. The system (A-1) can be written:

$$\begin{cases} \mathsf{V}\mathsf{X}_1 - \mathsf{B}\mathsf{X}_2 = \mu \mathsf{X}_1 \\ \mathsf{X}_1 = \mu \mathsf{X}_2 . \end{cases}$$

Multiplying the first equation by μ:

$$\mu\mathsf{V}\mathsf{X}_1 - \mu\mathsf{B}\mathsf{X}_2 = \mu^2 \mathsf{X}_1$$

and

$$\mathsf{V}\mu\mathsf{X}_1 - \mathsf{B}\mu\mathsf{X}_2 = \mu^2 \mathsf{X}_1$$

but $\mu\mathsf{X}_2 = \mathsf{X}_1$, therefore

$$\mathsf{V}\mu\mathsf{X}_1 - \mathsf{B}\mathsf{X}_1 = \mu^2 \mathsf{X}_1$$

which can be written:

$$(\mu^2 - \mathsf{V}\mu + \mathsf{B})\mathsf{X}_1 = 0 \qquad \text{(A-2)}$$

The last equation is entirely equivalent to the system (A-1): Therefore the eigenvalues are the same. It is also clear that the eigenvectors X_1 of (A-2) are the first $2n$ eigenvectors of (A-1).

References

BALTER, S., FELDMAN, R. & POST, B. (1971). *Phys. Rev. Lett.* **27**, 307–310.

COLE, H., CHAMBERS, F. W. & DUNN, H. M. (1962). *Acta Cryst.* **15**, 138–144.

COLELLA, R. (1972*a*). *Acta Cryst.* A**28**, 11–15.

COLELLA, R. (1972*b*). *Acta Cryst.* A**28**, 218.

DALISA, A. L., ZAJAC, A. & NG, C. H. (1968). *Phys. Rev.* **168**, 859–866.

EWALD, P. P. & HÉNO, Y. (1968). *Acta Cryst.* A**24**, 5–15.

FANKUCHEN, I. & EKSTEIN, H. (1949). Private communication quoted in Lipscomb (1949).

GOLDBERGER, M. L., LEWIS, H. W. & WATSON, K. M. (1963). *Phys. Rev.* **132**, 2764–2787.

HART, M. & LANG, A. R. (1961). *Phys. Rev. Lett.* **7**, 120–121.

HÉNO, Y. & EWALD, P. P. (1968). *Acta Cryst.* A**24**, 16–42.

HILDEBRANDT, G. (1967). *Phys. Stat. Sol.* **24**, 245–261.

JAMES, R. W. (1965). *The Optical Principles of the Diffraction of X-Rays*, Chap. VI, § 3. Cornell Univ. Press.

JEANS, J. (1933). *The Mathematical Theory of Electricity and Magnetism*, Chap. XVIII. Cambridge Univ. Press.

JOKO, T. & FUKUHARA, J. (1967). *J. Phys. Soc. Japan*, **22**, 597–604.

KAMBE, K. (1957). *J. Phys. Soc. Japan*, **12**, 13–25.

KARLE, J. (1964). *Advances in Structure Research by Diffraction Methods*, Vol. I, pp. 55–89, edited by R. BRILL. New York: Interscience.

KOTTWITZ, D. A. (1971). *Acta Cryst.* A**27**, 391–392.
LAMLA, E. (1939). *Ann. Phys.* (5) **36**, 194–208.
LIPSCOMB, W. N. (1949). *Acta Cryst.* **2**, 193–194.
PARAK, F., MÖSSBAUER, R. L., BIEBL, U., FORMANEK, H. & HOPPE, W. (1971). *Z. Phys.* **244**, 456–467.
PENNING, P. (1968). *Philips Res. Rep.* **23**, 12–24.
PENNING, P. & POLDER, D. (1968). *Philips Res. Rep.* **23**, 1–11.
RENNINGER, M. (1937). *Z. Phys.* **106**, 141–176.
RENNINGER, M. (1960). *Z. Kristallogr.* **113**, 99–103.
SACCOCIO, E. J. & ZAJAC, A. (1965). *Phys. Rev.* A**139**, 255–264.
WILLIAMSON, R. S. & FANKUCHEN, I. (1959). *Rev. Sci. Instrum.* **30**, 908–910.
ZACHARIASEN, W. H. (1945). *Theory of X-Ray Diffraction in Crystals.* New York: John Wiley.

Acta Cryst. (1974). A**30**, 423

Etude des Phases Haute Temperature de $NaNbO_3$ et des Correlations qui les Caracterisent*

BY F. DÉNOYER, R. COMÈS, M. LAMBERT ET A. GUINIER

Laboratoire associé au CNRS, Laboratoire de Physique des Solides, Université Paris-Sud, 91405-*Orsay, France*

(*Reçu le* 6 *octobre* 1973, *accepté le* 14 *novembre* 1973)

From the study of X-ray diffuse scattering diagrams, it has been shown that the diffuse scattering located along three equivalent reciprocal rods ⟨100⟩ in the cubic phase disappears successively at 641, 575 and 520°C. The interpretation is given in terms of planar local order.

Introduction

Parmi les perovskites, $NaNbO_3$ présente l'intérêt tout particulier de subir de nombreuses transitions de phase structurales, correspondant à des états paraélectriques, antiferroélectriques et ferroélectriques (Cross & Nicholson, 1955). Nous utiliserons ici la nomenclature des phases introduite par Lefkowitz, Lukaszewicz & Megaw, (1966), que nous reproduisons Tableau 1.

Les études par les méthodes classiques de détermination de structures ont donné les résultats suivants: au-dessus de 641 °C, les cristaux ont *la structure cubique du type perovskite*; les atomes de Na et de Nb sont situés respectivement au sommet et au centre du cube, alors que *les atomes d'oxygène aux centres des faces forment un octaèdre régulier*; récemment, Glazer & Megaw (1972) et Ahtee, Glazer & Megaw (1972) ont déterminé *les structures des phases* T_2, T_1 *et* S, stables respectivement entre 641 et 575, 575 et 520 et 520 et 480 °C. La symétrie moins élevée de ces différentes phases est conditionnée par *les rotations des atomes d'oxygène autour des axes* ⟨100⟩ *de l'octaèdre*. Ceci se traduit par un léger changement des paramètres de la maille cristalline.

Dans la phase T_2, de symétrie tétragonale, les atomes sont déplacés comme le montre la Fig. 1(*a*) par la rotation de l'octaèdre d'oxygène autour de l'axe **c** (Glazer & Megaw, 1972). A cette rotation, viennent s'ajouter celles autour de l'axe **a** dans la phase T_1, puis autour de l'axe **b** dans la phase S (Ahtee *et al.*, 1972). Les phases T_1 et S ont toutes deux la symétrie orthorhombique.

On voit sur les modèles A du Tableau 1 que *le déplacement de chacun des atomes de l'octaèdre d'oxygène résulte de deux rotations au maximum.*

Les structures qui viennent d'être décrites correspondent à *des structures moyennes*. La seule observation des réflexions de Bragg ne permet pas de décider si la structure de toutes les mailles est constante ou si elle fluctue d'une maille à l'autre, les fluctuations provenant du déplacement des atomes autour de leurs positions moyennes. C'est ainsi que le modèle B de la Fig. 2 est aussi valable que le modèle A pour expliquer l'ensemble des taches de diffraction du cristal. En effet, dans le modèle désordonné B, si l'atome d'oxygène occupe avec une égale probabilité les deux sites possibles, sa position moyenne n'est rien d'autre que celle déterminée dans la structure à périodicité parfaite [Fig. 2(*a*)].

Du point de vue des réflexions de Bragg, une répartition statistique des rotations dans un sens ou dans l'autre, (et) , autour de l'axe **a** (modèle B) introduit en fait un facteur d'atténuation par rapport à l'absence de rotation autour de cet axe (modèle A), mais ce facteur ne se traduira du point de vue expérimental que par une faible augmentation du facteur Debye–Waller très difficile à déceler.

Seule l'intensité diffusée en dehors des réflexions de Bragg peut nous renseigner de façon précise sur un tel désordre, qu'il soit statique ou dynamique.

L'objet de cet article est de montrer, à partir de *l'étude des diffusions 'anormales' de rayons X, que la phase cubique et les phases* T_2 *et* T_1 *sont 'désordonnées'*, que les modèles I_A, II_A et III_A doivent être respectivement

* Cet article fait partie du travail de la thèse de doctorat ès-sciences physiques de F. Dénoyer, enregistrée au CNRS sous le N° A.O. 9547.